

1 This is an accepted manuscript of an article published in Graefe's Archive for Clinical and  
2 Experimental Ophthalmology on 5<sup>th</sup> July 2020, available online. [https://doi.org/10.1007/s00417-020-](https://doi.org/10.1007/s00417-020-04820-7)  
3 04820-7

4

5 **Longitudinal outcomes of circumlimbal suture model induced**  
6 **chronic ocular hypertension in Sprague-Dawley albino rats**

7 Yamunadevi LAKSHMANAN<sup>1</sup>, Francisca Siu Yin WONG<sup>1</sup>, Bing ZUO<sup>2</sup>, Bang Viet BUI<sup>3</sup>, Henry Ho-  
8 Lung CHAN<sup>1,2</sup>

9 <sup>1</sup>Laboratory of Experimental Optometry (Neuroscience), School of Optometry, The Hong Kong  
10 Polytechnic University, Hong Kong SAR

11 <sup>2</sup>Centre for Myopia Research, School of Optometry, The Hong Kong Polytechnic University, Hong  
12 Kong SAR, China

13 <sup>3</sup>Department of Optometry and Vision Sciences, University of Melbourne, Melbourne, Australia

14

15 **\*Corresponding author:**

16 **Dr. Henry H.L. Chan,**

17 ORCID No: 0000-0002-8516-4711

18 E-mail: [henryhl.chan@polyu.edu.hk](mailto:henryhl.chan@polyu.edu.hk)

19 **Acknowledgement:**

20 The authors would like to thank Dr. Hsin-Hua Liu, Centre for Eye Research, Australia for sharing  
21 surgical technic nuances on model induction. The authors acknowledge Dr. Ricky Wing Kei WU,  
22 School of Medical and Health Sciences, Tung Wah College, Hong Kong for availing their laboratory  
23 facilities to perform the histological procedures. The authors also thank the University Research  
24 Facilities in Behavioral and Systems Neuroscience (UBSN) and in Life Sciences (ULS), The Hong  
25 Kong Polytechnic University for technical and facility supports.

## 26 **Abstract:**

### 27 **Purpose:**

28 To characterise longitudinal structural and functional changes in albino Sprague-Dawley rats following  
29 circumlimbal suture ocular hypertension (OHT) induction.

### 30 **Methods:**

31 Ten-week-old rats ( $n = 24$ ) underwent suture implantation around the limbal region in both eyes. On  
32 the next day, the suture was removed from one eye (control eyes) and left intact in the other eye  
33 (OHT eyes) of each animal. Intraocular pressure (IOP) was monitored weekly twice for the next 15  
34 weeks. Optical coherence tomography (OCT) and electroretinogram (ERG) were measured at  
35 baseline and weeks 4, 8, 12, and 15, and eyes were then collected for histological assessment.

### 36 **Results:**

37 Sutured eyes ( $n = 12$ ) developed IOP elevation of  $\sim 50\%$  in the first 2 weeks that was sustained at  $\sim$   
38  $25\%$  above the control eye up to week 15 ( $p = 0.001$ ). Animals with insufficient IOP elevation ( $n = 6$ ),  
39 corneal changes ( $n = 3$ ), and attrition ( $n = 3$ ) were excluded from the analysis. OHT eyes developed  
40 significant retinal nerve fibre layer (RNFL) thinning (week 4:  $-19 \pm 14\%$ ,  $p = 0.10$ ; week 8:  $-17 \pm$   
41  $12\%$ ,  $p = 0.04$ ; week 12:  $-16 \pm 10\%$ ,  $p = 0.04$ , relative to baseline) and reduction in retinal ganglion  
42 cell (RGC) density ( $-32 \pm 26\%$ ,  $p = 0.02$ ). At week 15, both inner ( $9 \pm 7\%$ ,  $p = 0.01$ ) and outer retinal  
43 layer thicknesses ( $6.0 \pm 5\%$ ,  $p = 0.001$ ) showed a mild increase in thicknesses. The positive scotopic  
44 threshold response ( $-28 \pm 25\%$ ,  $p = 0.04$ ) and a-wave were significantly reduced at week 12 ( $-35 \pm$   
45  $21\%$ ;  $p = 0.04$ ), whereas b-wave was not significantly affected (week 12:  $-18 \pm 27\%$ ,  $p = 0.24$ ).

### 46 **Conclusion:**

47 The circumlimbal suture model produced a chronic, moderate IOP elevation in an albino strain that  
48 led to RNFL thinning and reduced RGC density along with the reductions in ganglion and  
49 photoreceptor cell functions. There was a small thickening in both outer and inner retinal layers.

50 **Keywords:** Glaucoma, Intraocular pressure, Ocular hypertension, Animal model, Circumlimbal  
51 suture, Albino rat

## 52 **Introduction:**

53 Glaucoma is a blinding disease which is predicted to affect 76 million people worldwide by 2020 [1]  
54 with 11.2 million people presenting with bilateral blindness [2]. Increased intraocular pressure (IOP) is  
55 the major risk factor and the only modifiable factor in the current management of glaucoma [3,4].  
56 While IOP lowering delays disease progression, some patients continue to show vision loss despite  
57 well controlled IOP [3-5]. Thus, there remains a need to better understanding the pathogenesis of  
58 glaucoma. In this respect, animal models of glaucoma provide a means to study the disease  
59 mechanisms as well as to test novel treatment approaches.

60 Various animal models have been developed for studying glaucoma, including those in non-human  
61 primates, dogs, rodents, zebra fish, rabbits, sheep, cows, and birds [6]. Rodents are currently in wide  
62 spread use due to their low cost, effortless handling, ease of IOP measurement in awake animals and  
63 availability of various approaches to induce ocular hypertension (OHT) [7]. To simulate closed and  
64 open angle glaucoma types, OHT models aim to obstruct aqueous outflow either at, before or after  
65 the trabecular meshwork [8]. This can be achieved via intracameral injection of materials (e.g.  
66 microbeads) into the anterior chamber [9-11], laser photocoagulation of the trabecular meshwork [12-  
67 14] and/or limbal episcleral veins [15,16], injection of hypertonic saline into episcleral vein [17] and  
68 cauterization of episcleral veins [18]. Such models mimic certain aspects of glaucoma and are  
69 generally reproducible in rodents; however each has its own limitations. Thus, factors to consider  
70 when choosing a model of glaucoma include the invasiveness of the procedure, the need for repeated  
71 interventions, the presence of excessive secondary inflammation and anterior segment changes that  
72 impact imaging and whether there is a need for specialised instruments or training.

73 Recently, a circumlimbal suture model was developed to induce chronic OHT in rodents [19]. It is a  
74 simple and inexpensive approach that can be applied as a single intervention and facilitates  
75 longitudinal structural and functional assessments. In addition, the model allows lowering of IOP  
76 possible by simply removing the suture at different time points which assists in studying the recovery  
77 of neuronal dysfunction or structural preservation [20,21]. While this model was well characterized in  
78 pigmented strains [19,22,23], the effect of suture induced chronic IOP elevation in albino rat strains  
79 remains unknown. Albino rats are often used for OHT model induction to study the effect of IOP  
80 elevation on neuronal degeneration [9,12,14,16,18,24-26] and to test the efficacy of IOP lowering or

81 neuroprotective therapies on RGC survival [15,27-31]. Previously, two independent studies from the  
82 same laboratory revealed that suture model induction in albino CD-1 mice [32] could develop only  
83 moderate IOP elevation (~30%) sustaining for 2 weeks as compared with C57 pigmented mice [22]  
84 that produced relatively higher magnitude of IOP elevation (~70%) for 12 weeks. Despite moderate  
85 and brief period of IOP elevation, CD-1 developed RNFL thinning earlier than C57 mice. Thus, we  
86 hypothesise the circumlimbal suture model induction in albino rat strain may exhibit differential  
87 outcomes in terms of magnitude of IOP elevation, onset of retinal structure-function changes and its  
88 rate of progression. In this study, we sought to use Sprague-Dawley albino rat strain to investigate the  
89 effect of circumlimbal suture induced chronic IOP elevation on longitudinal retinal structure using *in*  
90 *vivo* optical coherence tomography (OCT) imaging and histology, and functional changes by  
91 electroretinogram (ERG).

92

## 93 **Materials and methods:**

### 94 **Animals**

95 Adult albino female Sprague-Dawley (SD) rats of 10 weeks old (180-210 grams) were housed in  
96 12:12 light/dark cycle lighting environment (200 lux maximum). Food (PicoLab® diet 20 (5053), PMI  
97 Nutrition International, Richmond, IN, USA) and water were available *ad libitum*. All experimental  
98 procedures and care involving the animals adhered to the ARVO Statement for the Use of Animals in  
99 Ophthalmic and Vision Research. The study was approved by The Animal Ethics-subcommittee of  
100 The Hong Kong Polytechnic University.

### 101 **Experimental design and OHT induction**

102 Twenty-four 10 week-old SD rats underwent OHT induction. Following baseline ERG and OCT  
103 measurements, all animals were acclimatised for 3 days to awake IOP measurements using a  
104 rebound tonometer (Tonolab, Icare, Vantaa, Finland). Baseline IOP was determined by averaging IOP  
105 measurements collected on two subsequent days. Each IOP measurements were average of 5  
106 reliable readings and the measurements were taken between 10:30 AM to 12:30 PM to avoid diurnal  
107 variations. On the day of OHT induction, animals were anesthetized with a mixture of 60 mg/kg

108 Ketamine and 5 mg/kg Xylazine (Alfasan International B.V, Woerden, Holland) via intraperitoneal  
109 injection. Following the application of a drop of topical anaesthetic (Provain-POS 0.5% w/v eye drop;  
110 URSAPHARM, Saarbrücken, Germany), both eyes underwent suture application. A suture (8/0 nylon)  
111 was applied around the globe at approximately 1.5 - 2 mm behind the limbus. The suture was secured  
112 using 6 to 7 subconjunctival anchor points as reported [19] with care taken to avoid the compression  
113 of the major episcleral veins. The suture was then tightened with a slipknot until IOP reached 60-70  
114 mmHg. The leftover suture was trimmed to prevent it from rubbing against the cornea. Eyes were  
115 then treated with a topical antibiotic eye drops, Gentamycin (Gibco, Thermo-Fisher Scientific,  
116 Waltham, MA, USA). To prevent the corneal dehydration during recovery from anaesthesia, Lacryvisc  
117 gel (Alcon, Rueil-Malmaison, France) was applied.

118 At post-operative day one, the suture was removed from one eye (control) and left intact in the other  
119 randomly chosen eye (suture). IOP was monitored on alternate days for the first week and twice a  
120 week thereafter until week 15. Sutured eyes that maintained an IOP elevation of 25% above their  
121 fellow control eyes (suture removed) during the first week were considered to be successful (OHT  
122 eye) and were followed up till week 15. Optical coherence tomography (OCT) imaging and  
123 electroretinogram (ERG) assessment was undertaken at 4, 8, 12 and 15 weeks after OHT induction.  
124 The changes in the retinal structure and function in the OHT eyes relative to the control eyes were  
125 determined. To ascertain the changes in OHT eyes were mainly induced by chronic IOP elevation  
126 instead of the initial IOP spike observed, a similar duration of IOP spike was induced in the control  
127 eyes by leaving the suture intact for a day. As animals required sedation for suture removal, the  
128 procedure was scheduled on the next day to avoid repeated anaesthesia within the same day.

129 Animals that had insufficient IOP elevation ( $n = 6$ ; less than 25% of fellow eye) in the first two weeks  
130 of OHT induction were not further assessed. Moreover, animals that developed corneal changes ( $n =$   
131  $3$ ; 12%) and attrition ( $n = 3$ , 12% of rats failed to recover from general anaesthesia during ERG/OCT  
132 measurements) were excluded from final analysis. Twelve rats completed the study and were  
133 sacrificed to collect retinal samples for morphological examination at week 15.

### 134 **Optical Coherence Tomography**

135 Spectral domain OCT (SD-OCT) (Micron IV, Phoenix Research Lab, Pleasanton, CA, USA) was used  
136 to image the peri-papillary retina. OCT imaging and analysis were conducted as described in our

137 previous study [33]. Briefly, following Ketamine-xylazine anaesthesia, the pupils were dilated using  
138 Mydracyl 1% eye drops (Alcon-Couvreur, Puurs, Belgium). Lubricating gel was applied on the  
139 corneal surface to improve the contact between the eye and the objective lens. A circular B-scan with  
140 a radius of 0.51 mm, consisting of 1024 A-scans was used to image the retinal layers. The axial and  
141 transverse resolutions of these images were 1.8  $\mu\text{m}$  and 3.0  $\mu\text{m}$  respectively. Semi-automated  
142 segmentation algorithm (Insight software, Phoenix Research Lab) was applied to analyse the B-scan  
143 images to provide total retinal thickness (TRT), retinal nerve fiber layer thickness (RNFLT), inner  
144 retinal layer thickness (IRLT) and outer retinal layer thickness (ORLT). The TRT was measured from  
145 the RPE layer to the inner limiting membrane, the IRLT included the thicknesses of the inner plexiform  
146 and inner nuclear layer, and the ORLT was measured from the RPE to the outer plexiform layer. The  
147 mean thickness of each layer was determined by averaging 1024 data points that covered the  
148 circumference of the circle.

## 149 **Electroretinography**

150 The full field electroretinogram was recorded using a white LED light (Ganzfeld, Q450; RETI Animal,  
151 Roland Consult, Brandenburg an der Havel, Germany). ERG measurements and analyses were  
152 conducted as described in our earlier report [33]. Briefly, animals were dark adapted overnight for 12  
153 hours and were anaesthetised (Ketamine-xylazine mixture) prior to data acquisition. Eyes were dilated  
154 and a drop of lubricating gel was applied to prevent corneal drying. Responses were obtained using  
155 gold ring electrodes placed on the corneal surface of both eyes; needles electrodes inserted into the  
156 lateral canthi and base of the tail served as reference and ground electrodes, respectively. As chronic  
157 IOP elevation largely affects the RGCs, the positive scotopic threshold response (pSTR) was  
158 recorded as a surrogate measure for RGC functions [34] along with the traditional recording of mixed  
159 scotopic responses (a- and b-waves). The pSTR was recorded using a series of brief flash (pulse  
160 length of 2  $\mu\text{s}$ ) stimulation intensities ranging from -4.8 to -4.05  $\log \text{cd.s/m}^2$  in 0.15  $\log \text{cd.s/m}^2$  steps.  
161 Each stimuli response was the average of 30 responses with an interstimulus interval of 2 seconds.  
162 Scotopic (mixed rod and cone) responses were recorded using a single flash of 1.3  $\log \text{cd.s/m}^2$ . All  
163 signals were recorded with a band pass filter of 0.1-1000 Hz. The amplitudes and implicit time of  
164 pSTR, scotopic a- and b-wave responses were quantified.

## 165 **Retinal Histology**

166 After OCT and ERG measurements at week 15, animals were euthanized by CO<sub>2</sub> asphyxiation. The  
167 eye cups were collected and fixed overnight using 4% paraformaldehyde in PBS at room temperature.  
168 The tissues were dehydrated using graded ethanol and paraffin embedded. 5 μm sections parallel to  
169 the optic nerve were collected, stained with Hematoxylin and Eosin (H&E) and imaged using a light  
170 microscope at 200x magnifications (Nikon, Tokyo, Japan). Regions of 500 μm x 500 μm of the central  
171 (250 μm away from the scleral canal opening) and peripheral retina (250 μm away from the ora  
172 serrata) as well as the anterior angle and optic nerve head were selected for morphological analysis.  
173 Cell density in ganglion cell layer (GCL) (cells/mm) was calculated by manually counting the number  
174 of nuclei in the ganglion cell layer and divided it by the corresponding retinal length measured using  
175 ImageJ (National Institute of Health, Bethesda, MA, USA) as reported previously [33].

## 176 **Retina Immunohistochemistry:**

177 The retinal sections were de-paraffinized, blocked with serum and incubated with primary mouse anti-  
178 β-III-tubulin (1:1000, BioLegend, San Diego, CA, USA) at 4°C overnight. To visualize the signal, the  
179 retinal sections were then incubated with Alexa Fluor 488 goat anti-mouse IgG (1:500; Molecular  
180 Probes, Invitrogen, Carlsbad, CA, USA) and the cell nuclei were counterstained with 4'-6-diamidino-2-  
181 phenylindole (DAPI). A light microscope (Nikon, Tokyo, Japan) was used to image the stained  
182 sections at 200x magnifications. The β-III-tubulin positive cells from central retinal region of 500 μm x  
183 500 μm were manually counted and divided by the corresponding retinal length using ImageJ  
184 (National Institute of Health, Bethesda, MA, USA) to return the RGC density (cells/mm)[35].

## 185 **Statistical Analysis**

186 All analyses were performed using SPSS 23 (IBM Corp, Armonk, NY, USA). Data were normally  
187 distributed and thus presented as mean with standard deviation. Two-way repeated measures (RM)  
188 ANOVA was used to compare differences in IOP, OCT and ERG parameters between suture and  
189 fellow control eyes that were measured over time (baseline, post OHT induction week 4, 8, 12 and 15)  
190 with Bonferroni post-hoc correction. For cell density in GCL, a paired t-test was used to compare the  
191 difference between suture and fellow control eyes. Also, the rates of change in structural and  
192 functional parameters upon OHT induction in the suture eye were first expressed relative to their

193 fellow control eye ((suture-control)/control x 100) and then as a difference (%) from baseline [35]. The  
194 level of significance was set as  $p < 0.05$ .

195

## 196 **Results:**

### 197 **Circumlimbal suture model produced a moderate IOP elevation in SD rats**

198 Fig. 1a shows an illustration of circumlimbal suture secured around the rat eye. Fig. 1b shows the  
199 position of suture from one representative rat on the day of suture placement (day 0) and at post-  
200 operative weeks 4, 8 and 15. Twelve animals met the  $\geq 25\%$  criteria for IOP elevation throughout the  
201 15 weeks and were free of complications. Baseline IOP in sutured and fellow control eyes was  $11 \pm 1$   
202 mmHg. Immediately after securing the suture, IOP spiked to  $64 \pm 16$  mmHg. This changed iris colour  
203 from red to pale red. After 5 minutes of suture placement, IOP returned to  $40 \pm 15$  mmHg and the iris  
204 regained its red colour.

205 Fig. 1c shows that IOP in sutured eyes was significantly greater than fellow control eyes (Two-way  
206 RM ANOVA: Between eyes:  $p = 0.001$ ; interaction effect:  $p = 0.003$ ). Post-hoc analysis shows that this  
207 was significant for all weeks, except for weeks 9 ( $p = 0.07$ ) and 14 ( $p = 0.09$ ). The sutured eyes  
208 developed an IOP elevation of  $\sim 50\%$  greater than the fellow control eye during the first 2 weeks of  
209 study period (Control:  $12 \pm 1$  mmHg; Suture:  $18 \pm 4$  mmHg,  $p < 0.001$ ). Subsequently, the IOP was  
210 maintained at  $\sim 25\%$  of increase till the end of the study at week 15. Suture placement for one day in  
211 the control eyes did not affect the IOP levels over next 15 weeks, which remained similar to baseline.

### 212 **Effect of IOP elevation on OCT measured retinal layers thicknesses**

213 Fig. 2 illustrates segmented SD-OCT B-scans along with fundus photographs from a representative  
214 rat showing the longitudinal changes in sutured (Fig. 2a) and fellow control eye (Fig. 2b) from baseline  
215 to week 15. All layers including TRT, RNFLT, IRLT and ORLT showed a significant interaction  
216 between eyes over time (Two-way RM ANOVA: interaction:  $p = 0.001$ ). Baseline TRT was similar  
217 between eyes ( $p = 0.90$ ). Following suture placement, TRT showed a slight thinning at week 4 ( $-1.6 \pm$   
218  $2.3\%$ ,  $p = 0.03$ ) when compared with fellow control eyes. At week 12 ( $2.0 \pm 2.9\%$ ,  $p = 0.04$ ) and week  
219 15 ( $5.0 \pm 4.7\%$ ,  $p = 0.001$ ), TRT in sutured eyes was slightly thicker than fellow control eyes (Fig. 3a).

220 The RNFL in sutured eyes (Fig. 3b) was significantly thinner than fellow control eyes at weeks 4 ( $p =$   
 221 0.03), 8 ( $p = 0.03$ ) and 12 ( $p = 0.04$ ). The rate of RNFLT loss (Fig. 6a) at week 4 was  $-19 \pm 14\%$  of  
 222 fellow control ( $p = 0.10$ ). Significant loss was detected at weeks 8 ( $-17 \pm 12\%$ ,  $p = 0.04$ ) and 12 ( $-16 \pm$   
 223  $10\%$ ,  $p = 0.04$ ). As for IRLT and ORLT, both were similar in suture and control eyes at week 4; but  
 224 were significantly thicker ( $p < 0.05$ ) in sutured eyes from week 8 to the end of the study (Fig. 3c and  
 225 3d). At week 15, the IRLT and ORLT in sutured eyes were  $9 \pm 7\%$  ( $p = 0.01$ ) and  $6 \pm 5\%$  ( $p = 0.001$ )  
 226 thicker than the fellow control eyes, respectively.

### 227 **Effect of IOP elevation on ERG measured retinal functions**

228 Fig. 4 shows averaged pSTR and scotopic ERG traces of suture eyes compared with fellow control  
 229 eyes. The pSTR responses (Fig. 5a) of sutured eyes were significantly reduced at week 12 ( $p = 0.04$ )  
 230 with no further reduction at week 15 (Two-way RM ANOVA: between eyes:  $p = 0.27$ ; time effect:  $p =$   
 231  $0.01$ ; interaction:  $p = 0.07$ ). Scotopic b-wave responses (Fig. 5b) were not significantly different  
 232 between sutured and control eyes (Two-way RM ANOVA: between eyes:  $p = 0.52$ ; time effect:  $p =$   
 233  $0.65$ ; interaction:  $p = 0.35$ ). Similar to the pSTR, scotopic a-wave responses (Fig. 5c) of suture eye  
 234 dropped significantly at week 12 ( $p = 0.01$ ) with no further reduction at week 15 (Two-way RM  
 235 ANOVA: between eyes:  $p = 0.06$ ; time effect:  $p = 0.48$ ; interaction:  $p = 0.05$ ). The inner retinal (pSTR),  
 236 mid-retinal (b-wave) and outer retinal (a-wave) functional loss at week 12 were  $-28 \pm 25\%$ , ( $p = 0.04$ ),  
 237  $-18 \pm 27\%$  ( $p = 0.24$ ) and  $-35 \pm 21\%$  ( $p = 0.04$ ) respectively.

238 Table 1 gives the implicit time of pSTR, b-wave and a-wave responses of sutured and fellow control  
 239 eyes. There was no difference in pSTR implicit time between suture and fellow control eyes at all  
 240 time-points (Two-way RM ANOVA: between eye:  $p = 0.09$ ; time effect:  $p = 0.38$ ; interaction:  $p = 0.63$ ).  
 241 However, the scotopic b-wave (Two-way RM ANOVA: between eye:  $p = 0.05$ ; time effect:  $p = 0.10$ ;  
 242 interaction:  $p = 0.82$ ) and a-wave (Two-way RM ANOVA: between eye:  $p = 0.03$ ; time effect:  $p = 0.59$ ;  
 243 interaction:  $p = 0.03$ ) in sutured eyes were delayed at weeks 8 (b wave: control: 69.9 ms, suture: 74.1  
 244 ms,  $p = 0.03$ ) and 12 (a wave: control: 7.7 ms, suture: 8.2 ms,  $p = 0.01$ ), respectively.

245 A summary of the effects of IOP elevation on retinal structure (thickness of RNFL, IRL and ORL) and  
 246 function (pSTR, scotopic b- and a-wave responses) is shown in Fig. 6a and 6b, respectively.

## 247 **Effect of IOP elevation on GCL density and axonal arrangements**

248 Fig. 7 presents the H&E stained retinal cross section that shows no obvious change in retinal layers at  
249 both peripheral and central regions from a representative sutured (Fig. 7b, 7d) and its fellow control  
250 eye (Fig. 7a, 7c) at week 15. Quantification revealed that the cell density in the GCL in suture eyes  
251 were significantly reduced in both peripheral ( $-18 \pm 16\%$ ,  $p = 0.02$ ) and central ( $-16 \pm 12\%$ ,  $p = 0.02$ )  
252 retina as compared with fellow control eyes (Fig. 7e). Considering the presence of both RGC and  
253 amacrine cells in the GCL, the retinal sections were further stained with  $\beta$ -III-tubulin, a RGC specific  
254 marker. The RGC density determined from the central retina showed a significant reduction in the  
255 suture eyes ( $-32 \pm 25\%$ ,  $p = 0.02$ ) as compared with the fellow control eyes (Fig. 8b). Sutured eyes  
256 also showed evidence of disruption of axonal bundle organisation with cellular infiltrates in the optic  
257 nerve and posterior deformation of optic nerve head surface as compared with fellow control eyes  
258 (Fig. 9).

259

## 260 **Discussion:**

261 This study demonstrated that a circumlimbal suture model produced a moderate, sustained IOP  
262 elevation in albino SD rats. The magnitude of IOP elevation in sutured eyes ( $\sim 50\%$ ) was milder than  
263 pigmented Long-Evans rat reported in a previous study [19] in which IOP elevation was  $\sim 100\%$  above  
264 control eyes in the first 4 weeks, gradually dropping to  $\sim 60\%$  at week 15. A similar procedure in albino  
265 CD-1 mice [32] induced only a milder IOP elevation of ( $\sim 30\%$ ) that sustained for a maximum period of  
266 2 weeks as compared with pigmented C57 mice ( $\sim 70\%$ ) lasting for a period of 12 weeks [22]. The  
267 magnitude of IOP elevation following suture implantation appears to be relatively lower in albino  
268 strains than pigmented ones. To ensure IOP measurements in the present study were not affected by  
269 any corneal changes induced by circumlimbal suture, we showed that IOP readings with the rebound  
270 tonometer were in good correlation with manometric IOP measurements in sutured SD rat eyes ( $n =$   
271 5) (Online Resource 1). Consistent with the previous study [19], no structural differences between the  
272 anterior chamber angles of sutured and control eyes were detected in this study (Online Resource 2).  
273 These findings suggested that the circumlimbal suture model produced a moderate, chronic elevation  
274 of IOP in SD rats, without any observable structural changes in the anterior chamber angles.

275 On longitudinal evaluation, IOP elevation in albino SD rats produced a significant RNFL thinning as  
276 early as week 4 and a corresponding decrease in pSTR response at week 12. As both eyes received  
277 the initial IOP spike, the changes in the retinal structure and function quantified in the experimental  
278 eyes with respect to control eyes were mainly driven by cumulative IOP over 15 weeks but not by the  
279 initial IOP spike. With regard to structure-function relationship, SD rats developed an early RNFL  
280 thinning (week 4) that did not progress beyond week 8, whereas pSTR amplitude continued to decline  
281 from week 8 to 12. The RNFL thinning appeared to precede pSTR attenuation could be due to greater  
282 inter-animal variability for the ERG results which make significant changes harder to detect.

283 Alternatively, IOP induced changes in membrane stretch sensitive channels (transient receptor  
284 potential vanilloid 1 expression) may transiently increase the magnitude of responses from retinal  
285 ganglion cells [36,37], thus increasing the pSTR response [38]. Under similar OHT induction, albino  
286 CD-1 mice [32] was also reported to show an early onset of RNFL loss and a severe thinning as  
287 compared with pigmented C57BL6/J [22], however functional assessment was not undertaken in this  
288 strain [32]. On the other hand, pigmented Long-Evans rats showed an earlier decline in the ganglion  
289 cell function (around week 2 to 4) that produced no further loss; but the RNFL exhibited a gradual and  
290 progressive thinning (from week 8 to 15). Consistent with RNFL thinning, the sutured eyes of SD rats  
291 showed a significant reduction in cell density in the GCL that was comparable with the quantification  
292 using RGC specific biomarker. While the retinal whole mount quantification of RGC was not  
293 performed in the present study, earlier studies reported that the RGC density estimated from retinal  
294 cross-sections were comparable to the whole mounted retina [39] or H&E stained GCL density [40] in  
295 models of optic nerve injury. Elevated IOP induced changes including altered arrangements of axon  
296 bundles, clustered nuclei of cellular infiltrates, which are suggestive of activated microglia [41-43] in  
297 the optic nerve and a posterior tissue displacement of the optic nerve head, were observed.

298 As for TRT, whilst the sutured eyes showed a mild increase over time, it was thinned in fellow control  
299 eyes (week 15:  $-8.0 \pm 1\%$ ) over 15 weeks of experimentation. We also observed a similar trend of  
300 thinning in naïve animals (Online Resource 3); thus possibly excluding the role of initial IOP spike in  
301 control eye could have resulted in the gradual decrease in TRT. These finding corroborated with our  
302 previous study, where there were no differences in OCT-measured retinal thicknesses between eyes  
303 receiving one day of OHT eyes and the fellow control eyes [35]. Using histological measurements,  
304 Chaychi et al. [44] reported a reduction in the thickness of photoreceptor layer, inner retinal layer

305 (INL, IPL) and RNFL in normal SD rats between P100 (age equivalent to week 8 follow up in the  
306 present study) to P300. Thus, the reduction in thickness in control eyes could be attributed to normal  
307 ageing. Using fellow eyes as controls should account for changes due to ageing and biometric  
308 changes over time.

309 Distinct from other suture studies, both outer (from RPE to OPL) and inner retinal layers (from IPL to  
310 INL) of OHT eyes showed a mild increase in thickness from week 8 to week 15 which was associated  
311 with a- and b-wave loss between weeks 8 and 12 (a-wave:  $-35 \pm 21\%$ ; b-wave:  $-18 \pm 27\%$ ). At week  
312 15, a small rebound was noticed in the ERG components (a-wave:  $-21 \pm 32\%$ ; b-wave:  $-12 \pm 34\%$ ). In  
313 pigmented strains, a non-progressive a-wave reduction was observed with no obvious change in ORL  
314 thickness [19,22]. The decrease in a-wave in the present study may have arisen from compromised  
315 choroidal blood flow to the outer retina, either from direct IOP elevation or indirectly from suture  
316 compressing the scleral and episcleral plexus. Such reductions in a- and b-wave responses has been  
317 reported in other experimental OHT models such as laser photocoagulation of episcleral and limbal  
318 veins [16] (SD rats: a-wave:  $-45\%$ ; b-wave:  $-35\%$  at Week 8) and cauterization of episcleral veins  
319 (Wistar rats: a-wave:  $-30\%$ ; b-wave:  $-25\%$  at Week 8) [24,45]. Also, a gradual and progressive  
320 reduction in the a-wave (7 months of age) followed by b-wave attenuation (8-9 months of age) has  
321 been also reported in the DBA/2Nnia glaucoma model [46]. This outer retinal deficit is thought to arise  
322 from reduction in choroidal blood flow, which was detectable at 4 months of age in DBA/2J mice,  
323 whereas retinal blood flow deficits were not noted until 6-9 months of age [47]. Previous report  
324 showed that suture implantation in C57 mice for 12 weeks did not cause any change in retinal blood  
325 flow (OCT Doppler) [23]. Considering the decrease in scotopic response and the change in ORL  
326 thickness in the present study, further investigations are warranted to investigate the possible role of  
327 ischemia with circumlimbal suture placement in SD rats. On the other hand, photoreceptor swelling  
328 has been reported previously in human glaucoma (post-mortem donor eyes) and in non-human  
329 primate model [48]. Furthermore, Choi et al. [49] showed a loss in cone density among glaucoma  
330 subjects of varying severity when imaged using adaptive optics. While the outer retinal changes in  
331 glaucoma remains largely equivocal, an underlying secondary vascular cause could possibly be  
332 overlooked. Interestingly, Wilsey et al. [50] also reported a thickening of the outer retinal complex ( $\sim 4$   
333 to  $5\%$ ) in non-human primate experimental glaucoma model (laser photocoagulation of TM) measured  
334 by OCT. Consistent with these findings, the present study also observed a relative increase in ORLT

335 from week 8 ( $2 \pm 1\%$ ) to week 15 ( $6 \pm 1\%$ ), possibly arising from changes in the photoreceptor layer  
336 following IOP elevation. However, this interpretation warrants thorough investigation.

337 It is worth noting that IOP elevation can alter axial length, which in turn affects the OCT  
338 measurements of retinal thicknesses (scan position and lateral magnification) [51]. We estimated the  
339 eyeball length from a subset of animals ( $n = 6$ ) after collecting the sample for histology. Sutured eyes  
340 showed an increase in eyeball length of 0.5 mm ( $7 \pm 3\%$ ) as compared to control eyes (Online  
341 Resource 4). An increase in axial length should result in a thinner retinal layer. However, the present  
342 study found TRT thickening (in particular ORL and IRL), and RNFL thinning. We speculate that the  
343 thickening of ORL may arise from compromised choroidal blood circulation, whereas IRL thickening  
344 may be related to glial cell proliferation [50,52,53].

345 The effect of suture induced chronic IOP on retinal structure (RNFL thickness, RGC density) and  
346 function (pSTR) reported in pigmented rodent strains [19,22] were also observed in the present study  
347 using SD rats. However, there appears to be a difference in the magnitude of IOP elevation and rate  
348 of structural and functional loss between strains. While adherence to surgical protocols and surgeon  
349 skills may likely affect the IOP induction, the present study adapted nearly all the surgical  
350 recommendations of suture model and was performed by a trained person. In this study, the distance  
351 of suture placement (2 mm from limbus) adapted was different from previous reports (1.5 mm from  
352 limbus) [19]. During our initial trials of model induction, sutures secured at a distance of 1.5 mm in SD  
353 rats was found to slip gradually towards the limbus over time, which could be attributed to the normal  
354 age-related increase in eyeball size in addition to the pressure exerted by the suture. This led to  
355 sudden IOP spikes and/or the development of corneal changes like steep cornea, cornea  
356 vascularization and opacity. All these adverse effects were subsequently reduced by securing the  
357 suture at a distance of 2 mm from the limbus. We further estimated the suture distance from limbus  
358 (SDL) posthumously for a subset of animals ( $n = 6$ ). The SDL did not influence the cumulative IOP ( $r$   
359  $= 0.32$ ;  $p = 0.53$ ), however it was inversely correlating with the ORLT ( $r = -0.84$ ,  $p = 0.04$ ) (Online  
360 Resource 5). As the SDL increased, the ORLT showed less thickening when compared with the  
361 control eyes, indicating that the choice of initial suture fixing distance at 2 mm away from limbus was  
362 less likely to induce outer retinal changes. However, the suture-encircling procedure, irrespective of  
363 suture placement distance, might still have influenced the choroidal blood supply as well as the outer

364 retinal structure and function. The RNFL was not showing progressive thinning in SD rats despite a  
365 significant loss at week 4. This may be due to the activation of glial cells, often detected during the  
366 process of neurodegeneration, masking the thinning of RNFL at later time points of the disease  
367 course [52,54]. Also, the magnitude of IOP elevation in the earlier weeks (~50% elevation) was not  
368 subsequently maintained in the later period (~25% elevation from week 4 to 12), which could possibly  
369 lower the rate of RNLF thinning after week 4. Although the current study did not use other strains, an  
370 earlier study reported strain specific difference in which albino mice (CD-1) manifested greater axonal  
371 and RGC loss following intracameral microbead injection as compared with other two pigmented  
372 mouse strains (C57, DBA/2J), despite all groups developed similar magnitudes of IOP elevation [10].  
373 Moreover, Bakalash et al. [55] reported a difference in susceptibility between two albino strains in  
374 which Lewis rat developed relatively greater RGC loss than SD rats when IOP was chronically  
375 elevated by laser photocoagulation of episcleral and limbal veins. The degree of IOP elevation and  
376 neuronal vulnerability between strains may be influenced by aqueous humour dynamics [56], scleral  
377 biomechanical properties [57] or immunological background [55,58] of different rodent strains. Thus  
378 strain specific neuronal susceptibility to stress [10,59-62] should be taken into account when  
379 comparing between studies. Besides, such differences between strains are in line with clinical  
380 scenario wherein patient responds distinctly to IOP stress (while some show resistance to IOP  
381 elevation, others are vulnerable to normal IOP levels) or progress at different rates to IOP elevation  
382 (while some progress at slower rate, others develop faster disease progression). Therefore, strain  
383 specific neuronal susceptibility can be advantageously utilized as models simulating various clinical  
384 conditions to study the disease pathogenesis and to test the efficacy of neuroprotective agents at the  
385 level of preclinical research [35,63].

386 In summary, following a single intervention, the circumlimbal suture OHT model in albino SD rats  
387 produced a moderate chronic IOP elevation that resulted in RNFL thinning and RGC loss. Also, the  
388 retinal function declined gradually over time thus providing a time window to test the effects of anti-  
389 glaucoma drugs, for example, the neuroprotective agents. However, SD rats also developed a small  
390 increase in both inner and outer retinal thicknesses. Over the course of the 15-week of  
391 experimentation, it was important to take into account age-related thinning of retinal layers. As the  
392 onset and the rate of structural and functional changes observed using SD rats differed from earlier

393 reports using pigmented strain, comparisons to other studies should take into account for strain  
 394 specific differences.

395

## 396 **Compliance with Ethical Standards:**

397 Funding: The study is supported by the General Research Fund (PolyU 151001/17M) from Research  
 398 Grants Council, HKSAR, Central Research Grant (for Research Student) and Internal Research  
 399 Grants (G-YBGC, Z0GF) from The Hong Kong Polytechnic University

400 Conflict of interest: The authors declare no conflict of interest.

401 Ethical approval: All applicable international, national, and/or institutional guidelines for the care and  
 402 use of animals were followed.

403

## 404 **References:**

- 405 1. Tham YC, Li X, Wong TY, Quigley HA, Aung T, Cheng CY (2014) Global prevalence of glaucoma and  
 406 projections of glaucoma burden through 2040: a systematic review and meta-analysis.  
 407 *Ophthalmology* 121 (11):2081-2090. doi:10.1016/j.ophtha.2014.05.013
- 408 2. Quigley HA, Broman AT (2006) The number of people with glaucoma worldwide in 2010 and 2020.  
 409 *Br J Ophthalmol* 90 (3):262-267. doi:10.1136/bjo.2005.081224
- 410 3. Heijl A, Leske MC, Bengtsson B, Hyman L, Bengtsson B, Hussein M, Early Manifest Glaucoma Trial  
 411 G (2002) Reduction of intraocular pressure and glaucoma progression: results from the Early  
 412 Manifest Glaucoma Trial. *Arch Ophthalmol* 120 (10):1268-1279. doi:10.1001/archophth.120.10.1268
- 413 4. Kass MA, Heuer DK, Higginbotham EJ, Johnson CA, Keltner JL, Miller JP, Parrish RK, Wilson MR,  
 414 Gordon MO (2002) The Ocular Hypertension Treatment Study: a randomized trial determines that  
 415 topical ocular hypotensive medication delays or prevents the onset of primary open-angle glaucoma.  
 416 *Arch Ophthalmol* 120 (6):701-713
- 417 5. Group CN-TGS (1998) Comparison of glaucomatous progression between untreated patients with  
 418 normal-tension glaucoma and patients with therapeutically reduced intraocular pressures. *Am J*  
 419 *Ophthalmol* 126 (4):487-497
- 420 6. Bouhenni R, Dunmire J, Sewell A, Edward DP (2012) Animal models of glaucoma. *BioMed Research*  
 421 *International* 2012:692609. doi:doi:10.1155/2012/692609
- 422 7. Johnson TV, Tomarev SI (2010) Rodent models of glaucoma. *Brain Res Bull* 81 (2-3):349-358
- 423 8. Vecino E, Sharma SC (2011) Glaucoma animal models. In: *Glaucoma-Basic and Clinical Concepts*.  
 424 IntechOpen, pp 319-334
- 425 9. Urcola JH, Hernández M, Vecino E (2006) Three experimental glaucoma models in rats:  
 426 comparison of the effects of intraocular pressure elevation on retinal ganglion cell size and death.  
 427 *Exp Eye Res* 83 (2):429-437

- 428 10. Cone FE, Gelman SE, Son JL, Pease ME, Quigley HA (2010) Differential susceptibility to  
429 experimental glaucoma among 3 mouse strains using bead and viscoelastic injection. *Exp Eye Res* 91  
430 (3):415-424
- 431 11. Sappington RM, Carlson BJ, Crish SD, Calkins DJ (2010) The microbead occlusion model: a  
432 paradigm for induced ocular hypertension in rats and mice. *Invest Ophthalmol Vis Sci* 51 (1):207-216
- 433 12. Levkovitch-Verbin H, Quigley HA, Martin KR, Valenta D, Baumrind LA, Pease ME (2002)  
434 Translimbal laser photocoagulation to the trabecular meshwork as a model of glaucoma in rats.  
435 *Invest Ophthalmol Vis Sci* 43 (2):402-410
- 436 13. Biermann J, van Oterendorp C, Stoykow C, Volz C, Jehle T, Boehringer D, Lagrèze WA (2012)  
437 Evaluation of intraocular pressure elevation in a modified laser-induced glaucoma rat model. *Exp Eye*  
438 *Res* 104:7-14
- 439 14. Ueda J, Sawaguchi S, Hanyu T, Yaoeda K, Fukuchi T, Abe H, Ozawa H (1998) Experimental  
440 glaucoma model in the rat induced by laser trabecular photocoagulation after an intracameral  
441 injection of India ink. *Jpn J Ophthalmol* 42 (5):337-344
- 442 15. WoldeMussie E, Ruiz G, Wijono M, Wheeler LA (2001) Neuroprotection of retinal ganglion cells  
443 by brimonidine in rats with laser-induced chronic ocular hypertension. *Invest Ophthalmol Vis Sci* 42  
444 (12):2849-2855
- 445 16. Li RS, Tay DK, Chan HH, So KF (2006) Changes of retinal functions following the induction of  
446 ocular hypertension in rats using argon laser photocoagulation. *Clin Experiment Ophthalmol* 34  
447 (6):575-583
- 448 17. Morrison JC, Moore C, Deppmeier LM, Gold BG, Meshul CK, Johnson EC (1997) A rat model of  
449 chronic pressure-induced optic nerve damage. *Exp Eye Res* 64 (1):85-96
- 450 18. Shareef S, Garcia-Valenzuela E, Salierno A, Walsh J, Sharma S (1995) Chronic ocular hypertension  
451 following episcleral venous occlusion in rats. *Exp Eye Res* 61 (3):379-382
- 452 19. Liu H-H, Bui BV, Nguyen CT, Kezic JM, Vingrys AJ, He Z (2015) Chronic ocular hypertension  
453 induced by circumlimbal suture in rats. *Invest Ophthalmol Vis Sci* 56 (5):2811-2820
- 454 20. Liu HH, He Z, Nguyen CT, Vingrys AJ, Bui BV (2017) Reversal of functional loss in a rat model of  
455 chronic intraocular pressure elevation. *Ophthalmic Physiol Opt* 37 (1):71-81
- 456 21. Zhao D, Wong VHY, He Z, Nguyen CTO, Jobling AI, Fletcher E, Chinnery H, Jusuf P, Lim JK, Vingrys  
457 AJ (2018) Reversibility of retinal ganglion cell dysfunction due to chronic IOP elevation. *Invest*  
458 *Ophthalmol Vis Sci* 59 (9):3696-3696
- 459 22. Liu H-H, Flanagan JG (2017) A mouse model of chronic ocular hypertension induced by  
460 circumlimbal suture. *Invest Ophthalmol Vis Sci* 58 (1):353-361
- 461 23. Zhao D, Nguyen CT, Wong VH, Lim JK, He Z, Jobling AI, Fletcher EL, Chinnery HR, Vingrys AJ, Bui  
462 BV (2017) Characterization of the circumlimbal suture model of chronic IOP elevation in mice and  
463 assessment of changes in gene expression of stretch sensitive channels. *Front Neurosci* 11:41
- 464 24. Bayer AU, Danias J, Brodie S, Maag KP, Chen B, Shen F, Podos SM, Mittag TW (2001)  
465 Electroretinographic Abnormalities in a Rat Glaucoma Model with Chronic Elevated Intraocular  
466 Pressure. *Exp Eye Res* 72 (6):667-677. doi:<https://doi.org/10.1006/exer.2001.1004>
- 467 25. Ben-Shlomo G, Bakalash S, Lambrou GN, Latour E, Dawson WW, Schwartz M, Ofri R (2005)  
468 Pattern electroretinography in a rat model of ocular hypertension: functional evidence for early  
469 detection of inner retinal damage. *Exp Eye Res* 81 (3):340-349. doi:10.1016/j.exer.2005.02.006
- 470 26. Kim DH, Kim HS, Ahn MD, Chun MH (2004) Ganglion cell death in rat retina by persistent  
471 intraocular pressure elevation. *Korean J Ophthalmol* 18 (1):15-22. doi:10.3341/kjo.2004.18.1.15
- 472 27. Chan HC, Chang RC, Koon-Ching Ip A, Chiu K, Yuen WH, Zee SY, So KF (2007) Neuroprotective  
473 effects of Lycium barbarum Lynn on protecting retinal ganglion cells in an ocular hypertension model  
474 of glaucoma. *Exp Neurol* 203 (1):269-273. doi:10.1016/j.expneurol.2006.05.031
- 475 28. Colafrancesco V, Parisi V, Sposato V, Rossi S, Russo MA, Coassin M, Lambiase A, Aloe L (2011)  
476 Ocular application of nerve growth factor protects degenerating retinal ganglion cells in a rat model  
477 of glaucoma. *J Glaucoma* 20 (2):100-108. doi:10.1097/IJG.0b013e3181d787e5

- 478 29. Hernández M, Urcola JH, Vecino E (2008) Retinal ganglion cell neuroprotection in a rat model of  
479 glaucoma following brimonidine, latanoprost or combined treatments. *Exp Eye Res* 86 (5):798-806.  
480 doi:<https://doi.org/10.1016/j.exer.2008.02.008>
- 481 30. Sarup V, McEwan GC, Thompson C, Patil KA, Sharma SC (2005) Dorzolamide and timolol saves  
482 retinal ganglion cells in glaucomatous adult rats. *J Ocul Pharmacol Ther* 21 (6):454-462.  
483 doi:10.1089/jop.2005.21.454
- 484 31. Seki M, Tanaka T, Matsuda H, Togano T, Hashimoto K, Ueda J, Fukuchi T, Abe H (2005) Topically  
485 administered timolol and dorzolamide reduce intraocular pressure and protect retinal ganglion cells  
486 in a rat experimental glaucoma model. *Br J Ophthalmol* 89 (4):504-507.  
487 doi:10.1136/bjo.2004.052860
- 488 32. Liu H-H, Zhang L, Shi M, Chen L, Flanagan JG (2017) Comparison of laser and circumlimbal suture  
489 induced elevation of intraocular pressure in albino CD-1 mice. *PLoS One* 12 (11):e0189094
- 490 33. Lakshmanan Y, Wong FS, Yu WY, Li SZ, Choi KY, So KF, Chan HH (2019) Lycium Barbarum  
491 Polysaccharides Rescue Neurodegeneration in an Acute Ocular Hypertension Rat Model Under Pre-  
492 and Posttreatment Conditions. *Invest Ophthalmol Vis Sci* 60 (6):2023-2033. doi:10.1167/iovs.19-  
493 26752
- 494 34. Bui BV, Fortune B (2004) Ganglion cell contributions to the rat full-field electroretinogram. *The*  
495 *Journal of physiology* 555 (1):153-173
- 496 35. Lakshmanan Y, Wong FSY, Zuo B, So K-F, Bui BV, Chan HH-L (2019) Posttreatment Intervention  
497 With Lycium Barbarum Polysaccharides is Neuroprotective in a Rat Model of Chronic Ocular  
498 Hypertension. *Invest Ophthalmol Vis Sci* 60 (14):4606-4618. doi:10.1167/iovs.19-27886
- 499 36. Weitlauf C, Ward NJ, Lambert WS, Sidorova TN, Ho KW, Sappington RM, Calkins DJ (2014) Short-  
500 term increases in transient receptor potential vanilloid-1 mediate stress-induced enhancement of  
501 neuronal excitation. *J Neurosci* 34 (46):15369-15381
- 502 37. Risner ML, Pasini S, Cooper ML, Lambert WS, Calkins DJ (2018) Axogenic mechanism enhances  
503 retinal ganglion cell excitability during early progression in glaucoma. *Proceedings of the National*  
504 *Academy of Sciences* 115 (10):E2393-E2402
- 505 38. Choh V, Gurdita A, Tan B, Prasad RC, Bizheva K, Joos KM (2016) Short-term moderately elevated  
506 intraocular pressure is associated with elevated scotopic electroretinogram responses. *Invest*  
507 *Ophthalmol Vis Sci* 57 (4):2140-2151
- 508 39. Mead B, Thompson A, Scheven BA, Logan A, Berry M, Leadbeater W (2014) Comparative  
509 Evaluation of Methods for Estimating Retinal Ganglion Cell Loss in Retinal Sections and  
510 Wholemounts. *PLoS One* 9 (10):e110612. doi:10.1371/journal.pone.0110612
- 511 40. Dheer Y, Chitranshi N, Gupta V, Sharma S, Pushpitha K, Abbasi M, Mirzaei M, You Y, Graham SL,  
512 Gupta V (2019) Retinoid x receptor modulation protects against ER stress response and rescues  
513 glaucoma phenotypes in adult mice. *Exp Neurol* 314:111-125.  
514 doi:<https://doi.org/10.1016/j.expneurol.2019.01.015>
- 515 41. Shindler KS, Guan Y, Ventura E, Bennett J, Rostami A (2006) Retinal ganglion cell loss induced by  
516 acute optic neuritis in a relapsing model of multiple sclerosis. *Multiple Sclerosis Journal* 12 (5):526-  
517 532. doi:10.1177/1352458506070629
- 518 42. Horstmann L, Schmid H, Heinen AP, Kurschus FC, Dick HB, Joachim SC (2013) Inflammatory  
519 demyelination induces glia alterations and ganglion cell loss in the retina of an experimental  
520 autoimmune encephalomyelitis model. *J Neuroinflammation* 10:120-120. doi:10.1186/1742-2094-  
521 10-120
- 522 43. Renner M, Stute G, Alzureiqi M, Reinhard J, Wiemann S, Schmid H, Faissner A, Dick HB, Joachim  
523 SC (2017) Optic Nerve Degeneration after Retinal Ischemia/Reperfusion in a Rodent Model. *Front*  
524 *Cell Neurosci* 11:254-254. doi:10.3389/fncel.2017.00254
- 525 44. Chaychi S, Polosa A, Lachapelle P (2015) Differences in retinal structure and function between  
526 aging male and female sprague-dawley rats are strongly influenced by the estrus cycle. *PLoS One* 10  
527 (8):e0136056

- 528 45. Mittag TW, Danias J, Pohorenc G, Yuan HM, Burakgazi E, Chalmers–Redman R, Podos SM,  
529 Tatton WG (2000) Retinal Damage after 3 to 4 Months of Elevated Intraocular Pressure in a Rat  
530 Glaucoma Model. *Invest Ophthalmol Vis Sci* 41 (11):3451-3459
- 531 46. Bayer AU, Neuhardt T, May AC, Martus P, Maag K-P, Brodie S, Lütjen–Drecoll E, Podos SM,  
532 Mittag T (2001) Retinal morphology and ERG response in the DBA/2Nnia mouse model of angle-  
533 closure glaucoma. *Invest Ophthalmol Vis Sci* 42 (6):1258-1265
- 534 47. Lavery WJ, Muir ER, Kiel JW, Duong TQ (2012) Magnetic resonance imaging indicates decreased  
535 choroidal and retinal blood flow in the DBA/2J mouse model of glaucoma. *Invest Ophthalmol Vis Sci*  
536 53 (2):560-564
- 537 48. Nork TM, Ver Hoeve JN, Poulsen GL, Nickells RW, Davis MD, Weber AJ, Sarks SH, Lemley HL,  
538 Millecchia LL (2000) Swelling and loss of photoreceptors in chronic human and experimental  
539 glaucomas. *Arch Ophthalmol* 118 (2):235-245
- 540 49. Choi SS, Zawadzki RJ, Lim MC, Brandt JD, Keltner JL, Doble N, Werner JS (2011) Evidence of outer  
541 retinal changes in glaucoma patients as revealed by ultrahigh-resolution in vivo retinal imaging. *Br J*  
542 *Ophthalmol* 95 (1):131-141
- 543 50. Wilsey LJ, Reynaud J, Cull G, Burgoyne CF, Fortune B (2016) Macular structure and function in  
544 nonhuman primate experimental glaucoma. *Invest Ophthalmol Vis Sci* 57 (4):1892-1900
- 545 51. Lozano DC, Twa MD (2013) Development of a rat schematic eye from in vivo biometry and the  
546 correction of lateral magnification in SD-OCT imaging. *Invest Ophthalmol Vis Sci* 54 (9):6446-6455
- 547 52. Hood DC, Lin CE, Lazow MA, Locke KG, Zhang X, Birch DG (2009) Thickness of receptor and post-  
548 receptor retinal layers in patients with retinitis pigmentosa measured with frequency-domain optical  
549 coherence tomography. *Invest Ophthalmol Vis Sci* 50 (5):2328-2336
- 550 53. Kim EK, Park H-YL, Park CK (2017) Relationship between retinal inner nuclear layer thickness and  
551 severity of visual field loss in glaucoma. *Sci Rep* 7 (1):5543
- 552 54. Choe TE, Abbott CJ, Piper C, Wang L, Fortune B (2014) Comparison of Longitudinal In Vivo  
553 Measurements of Retinal Nerve Fiber Layer Thickness and Retinal Ganglion Cell Density after Optic  
554 Nerve Transection in Rat. *PLoS One* 9 (11):e113011. doi:10.1371/journal.pone.0113011
- 555 55. Bakalash S, Kipnis J, Yoles E, Schwartz M (2002) Resistance of Retinal Ganglion Cells to an  
556 Increase in Intraocular Pressure Is Immune-Dependent. *Invest Ophthalmol Vis Sci* 43 (8):2648-2653
- 557 56. Bousso-Calleja A, Overby DR (2013) The Influence of Genetic Background on Conventional  
558 Outflow Facility in MiceStrain-Dependent Conventional Outflow Facility in Mice. *Invest Ophthalmol*  
559 *Vis Sci* 54 (13):8251-8258. doi:10.1167/iovs.13-13025
- 560 57. Nguyen C, Cone FE, Nguyen TD, Coudrillier B, Pease ME, Steinhart MR, Oglesby EN, Jefferys JL,  
561 Quigley HA (2013) Studies of Scleral Biomechanical Behavior Related to Susceptibility for Retinal  
562 Ganglion Cell Loss in Experimental Mouse GlaucomaScleral Biomechanical Behavior in Mouse  
563 Glaucoma. *Invest Ophthalmol Vis Sci* 54 (3):1767-1780. doi:10.1167/iovs.12-10952
- 564 58. Huang Y, Li Z, van Rooijen N, Wang N, Pang CP, Cui Q (2007) Different responses of macrophages  
565 in retinal ganglion cell survival after acute ocular hypertension in rats with different autoimmune  
566 backgrounds. *Exp Eye Res* 85 (5):659-666. doi:<https://doi.org/10.1016/j.exer.2007.07.020>
- 567 59. Dorfman AL, Polosa A, Joly S, Chemtob S, Lachapelle P (2009) Functional and structural changes  
568 resulting from strain differences in the rat model of oxygen-induced retinopathy. *Invest Ophthalmol*  
569 *Vis Sci* 50 (5):2436-2450
- 570 60. Gurdita A, Tan B, Joos KM, Bizheva K, Choh V (2017) Pigmented and albino rats differ in their  
571 responses to moderate, acute and reversible intraocular pressure elevation. *Documenta*  
572 *ophthalmologica Advances in ophthalmology* 134 (3):205-219. doi:10.1007/s10633-017-9586-x
- 573 61. Polosa A, Bessaklia H, Lachapelle P (2016) Strain differences in light-induced retinopathy. *PLoS*  
574 *One* 11 (6):e0158082
- 575 62. Safa R, Osborne NN (2000) Retinas from albino rats are more susceptible to ischaemic damage  
576 than age-matched pigmented animals. *Brain Res* 862 (1-2):36-42

577 63. Livne-Bar I, Wei J, Liu H-H, Alqawlaq S, Won G-J, Tuccitto A, Gronert K, Flanagan JG, Sivak JM  
 578 (2017) Astrocyte-derived lipoxins A 4 and B 4 promote neuroprotection from acute and chronic  
 579 injury. The Journal of clinical investigation 127 (12):4403-4414

580

## 581 **Tables:**

### 582 **Table 1**

583 **Implicit time of pSTR, scotopic b- and a-wave responses of the control and suture eyes**  
 584 **measured over 15 weeks.**

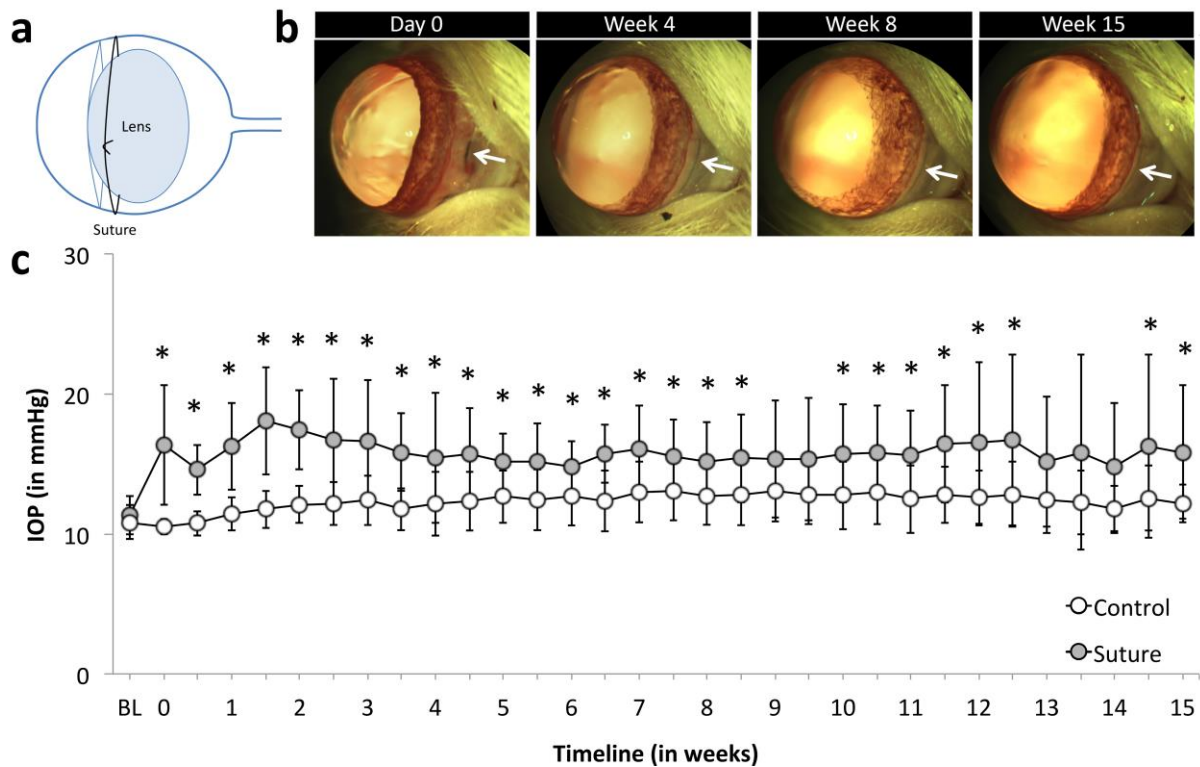
Implicit time (ms)	Eye	Baseline	Week 4	Week 8	Week 12	Week 15
<b>pSTR (SEM)</b>	Control	113.2 (2.7)	114.9 (3.4)	110.7 (1.8)	110.5 (2.7)	117.4 (2.4)
	Suture	114.2 (2.7)	115.1 (3.0)	113.9 (3.2)	113.7 (2.6)	119.3 (2.0)
<b>b-wave (SEM)</b>	Control	69.9 (2.0)	70.4 (1.9)	69.9 (2.4)	78.3 (4.5)	73.0 (1.9)
	Suture	73.2 (2.2)	73.2 (2.6)	74.2 (2.1)*	79.5 (3.1)	73.0 (2.3)
<b>a-wave (SEM)</b>	Control	8.0 (0.1)	7.8 (0.1)	7.7 (0.1)	7.8 (0.4)	7.7 (0.1)
	Suture	7.9 (0.1)	8.1 (0.1)	7.8 (0.1)	8.2 (0.3)†	7.9 (0.1)

585 \* p<0.05; † p<0.01 (\* † Bonferroni's post hoc test of Two-way RM ANOVA)

586

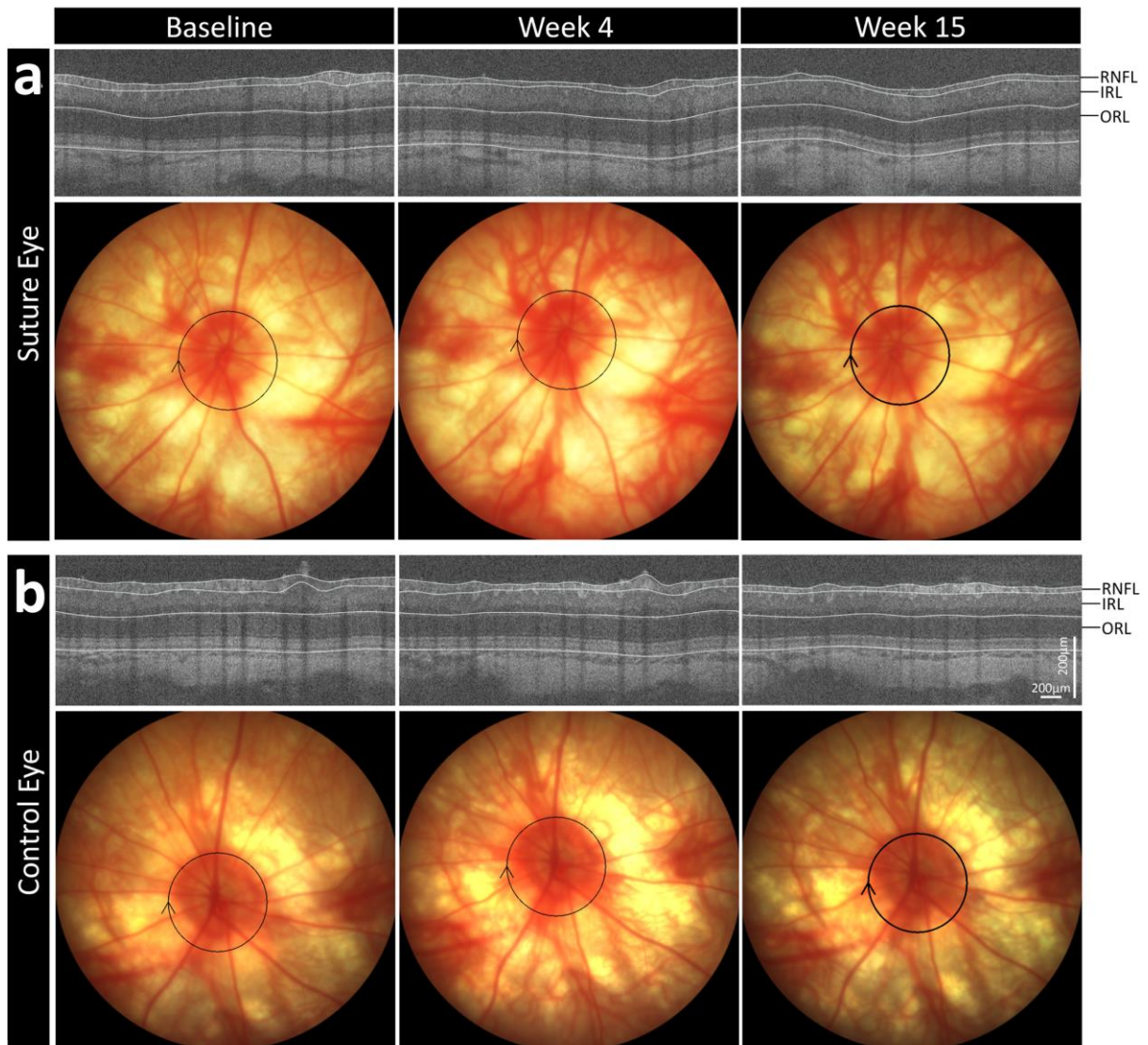
## 587 **Figures:**

588



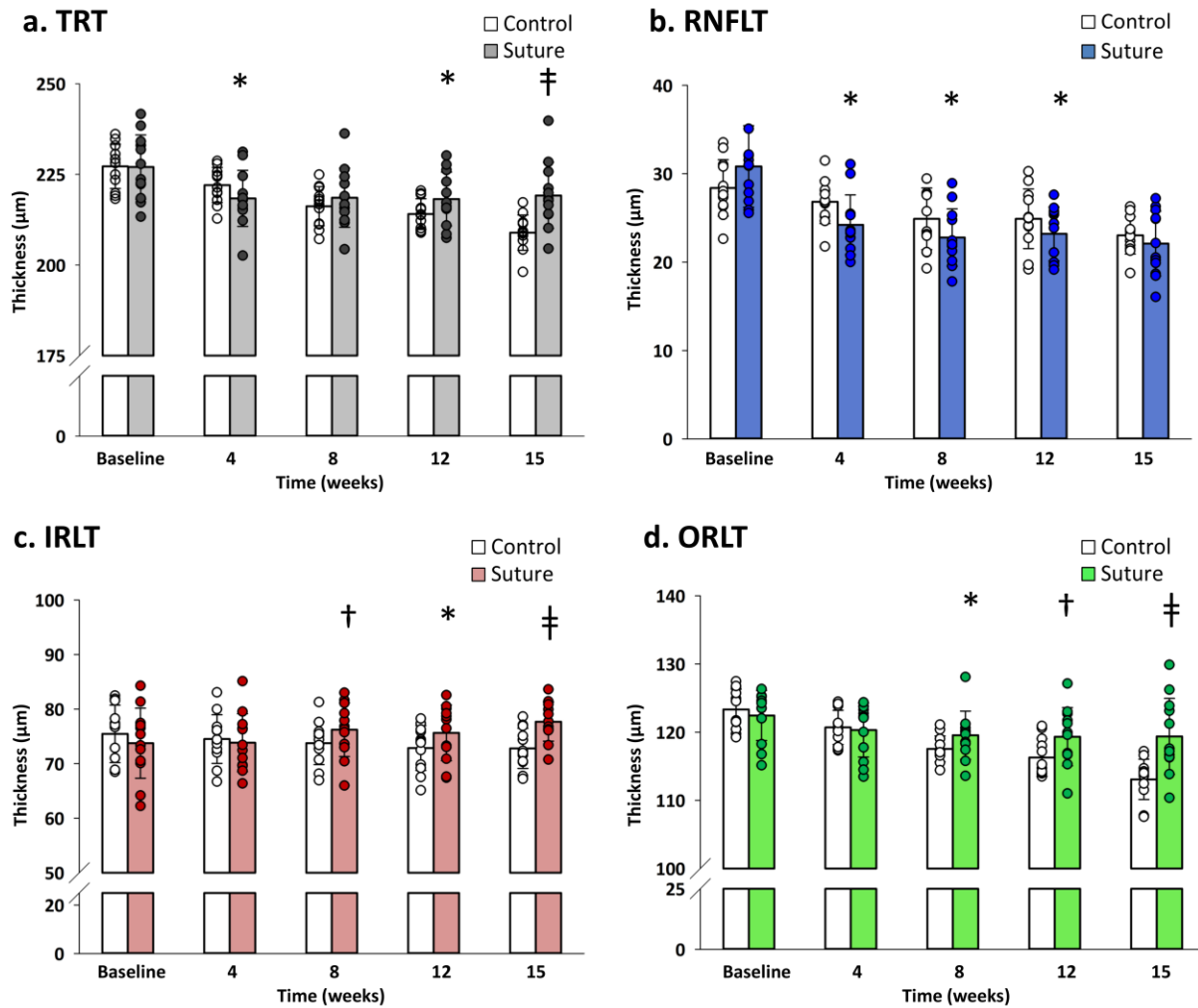
589 **Fig. 1** Chronic OHT induction was achieved by securing a suture firmly around the globe. (a) An  
 590 illustration of circumlimbal suture secured at a distance of ~1.5 to 2 mm behind the limbus in the rat  
 591 eye. (b) Suture positions from one representative rat at day 0 (10 minutes after suture placement) and  
 592 end of weeks 4, 8 and 15 (white arrow). (c) The circumlimbal suture induced a moderate and chronic  
 593 IOP elevation in albino rats (n = 12) for at least 15 weeks, while control eyes which had the suture  
 594 removed at day 1 showed stable IOP. Error bars: standard deviation. \* p < 0.05 (\* Bonferroni's post-  
 595 hoc test of Two-way RM ANOVA).

596



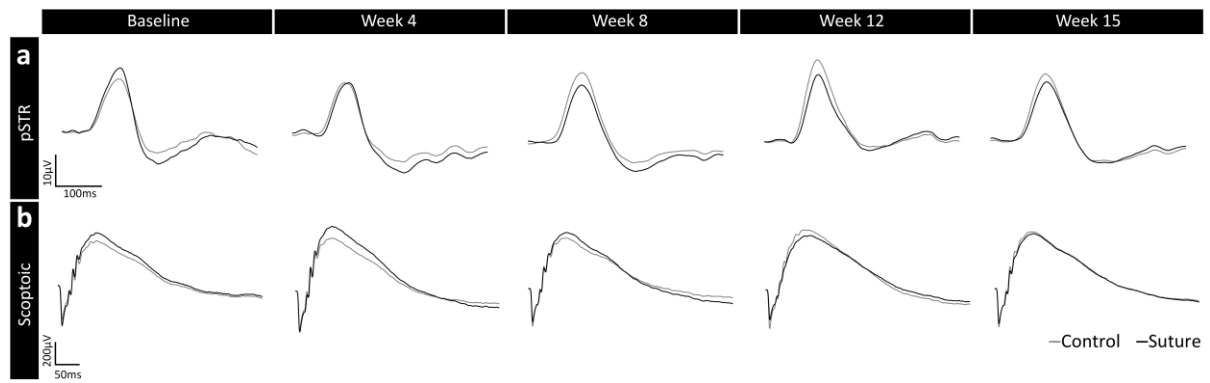
597 **Fig. 2** Peripapillary SD-OCT B-scan images and fundus photographs of (a) sutured eye (b) fellow  
 598 control of one representative rat taken at baseline, and after 4 and 15 weeks of IOP elevation. OCT  
 599 circle scan positions are indicated in black circle on their corresponding fundus photographs. OCT  
 600 images were segmented to determine RNFL, IRL and ORL thicknesses. RNFL, retinal nerve fibre  
 601 layer; IRL, inner retinal layer (includes inner plexiform and inner nuclear layer); ORLT, outer retinal  
 602 layer (from RPE to outer plexiform layer).

603



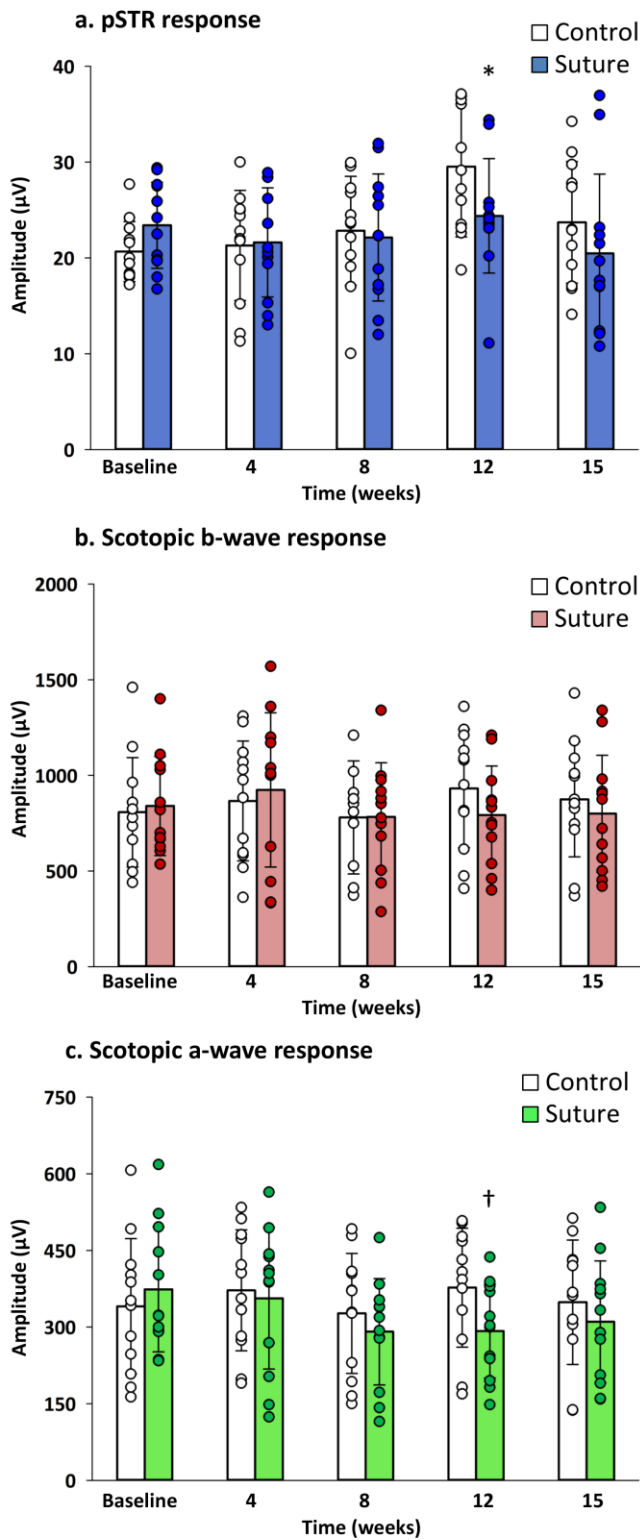
604 **Fig. 3** The effect of chronic IOP on OCT measured retinal thicknesses. The thicknesses of (a) TRT,  
 605 (b) RNFLT, (c) IRLT and (d) ORLT were compared between sutured and fellow control eyes (n = 12).  
 606 \* p < 0.05; † p < 0.01; ‡ p < 0.001 (\* † ‡ Bonferroni's post hoc test of Two-way RM ANOVA). Error  
 607 bars: standard deviation. Each circle in the bar chart represents individual data points of the animals.  
 608 TRT, Total retinal thickness; RNFLT, retinal nerve fibre layer thickness; IRLT, inner retinal layer  
 609 thickness; ORLT, outer retinal layer thickness

610



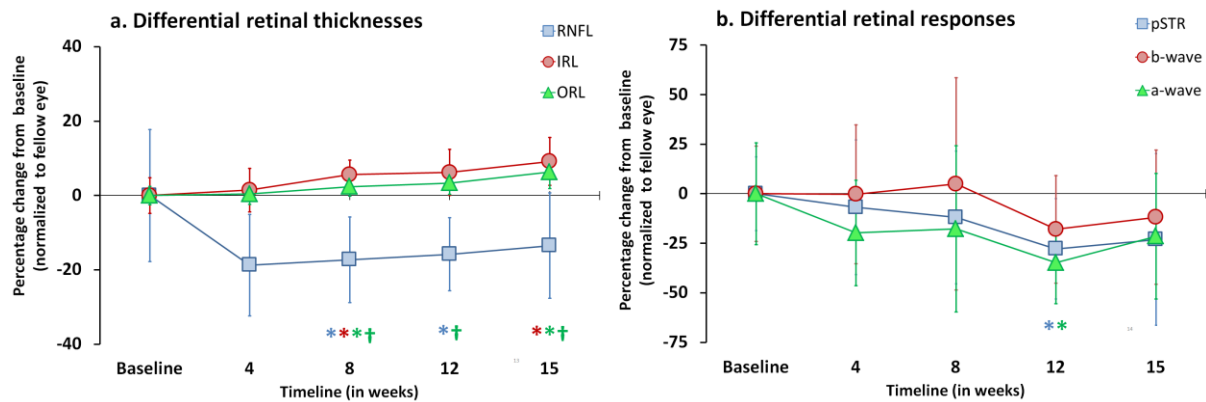
611 **Fig. 4** Changes in inner and outer retinal responses over the 15 weeks of IOP elevation: (a) pSTR  
 612 and (b) scotopic ERG. Black and gray traces represent averaged responses from suture and control  
 613 eyes (n = 12) respectively.

614



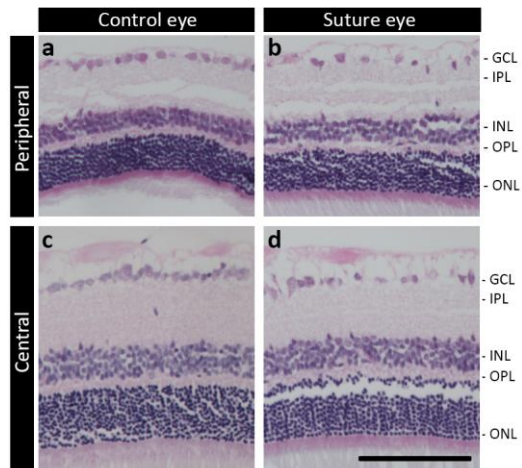
615 **Fig. 5** The effect of chronic IOP on ERG measured retinal functions. The responses of ganglion,  
 616 bipolar and photoreceptor cell responses were presented as (a) pSTR, (b) b-wave and (c) a-wave  
 617 respectively (n = 12). Error bars: standard deviation. Each circle in the bar chart represents individual  
 618 data points of the animals. \* p < 0.05; † p < 0.01; (\* † Bonferroni's post-hoc test of Two-way RM  
 619 ANOVA). pSTR, positive scotopic threshold responses.

620

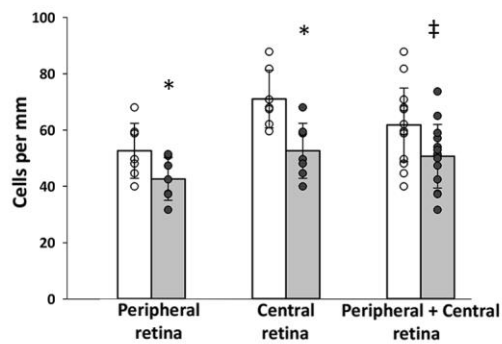


621 **Fig. 6** The effect of chronic IOP on retinal structure and function were summarised as percentage  
 622 change from fellow control eyes. (a) Thicknesses of RNFL (retinal nerve fiber layer), IRL (inner retinal  
 623 layer) and ORL (outer retinal layer) measured by OCT and (b) their complementary functional  
 624 measurements, pSTR (positive scotopic threshold responses), scotopic b- and a-wave responses  
 625 determined by ERG. Error bars: standard deviation. \*  $p < 0.05$  vs. baseline; †  $p < 0.05$  vs. week 4; (\* †  
 626 Bonferroni's pos- hoc test of RM ANOVA).

627

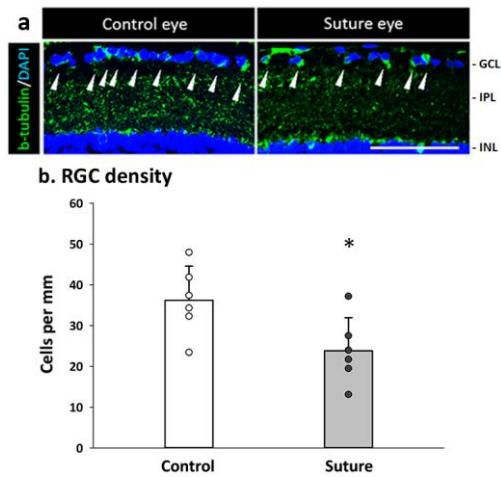


e. Cell density in Ganglion cell layer



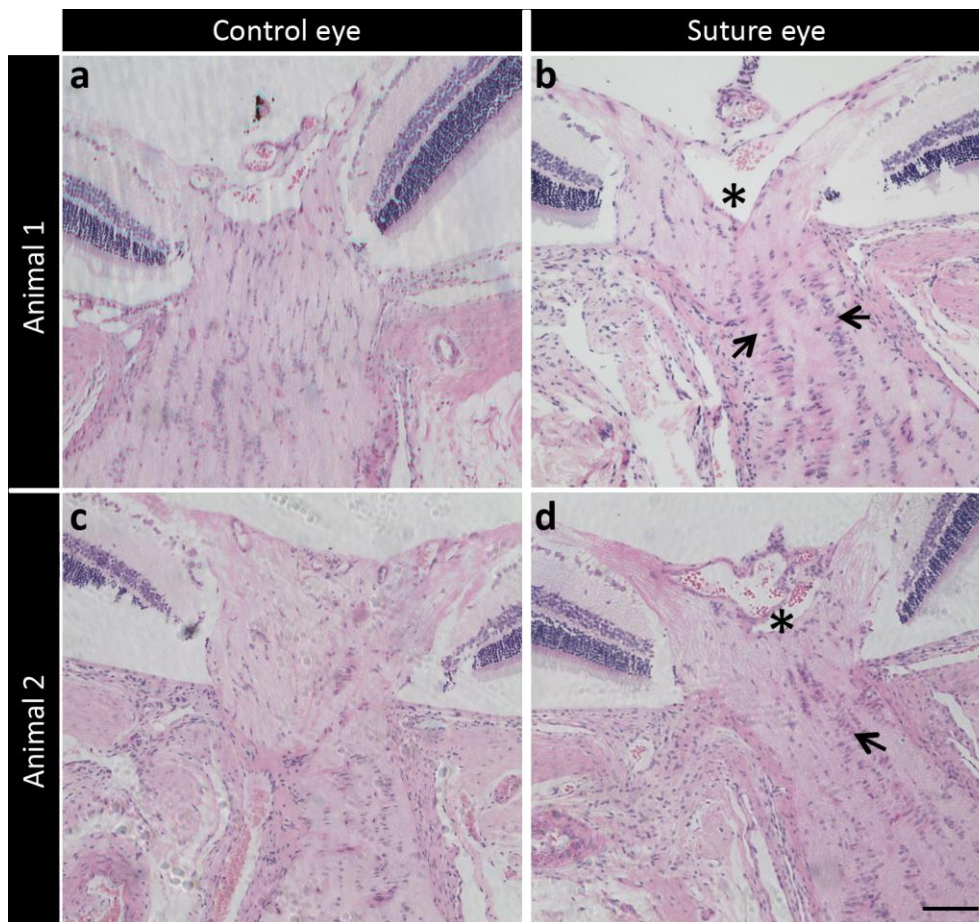
628 **Fig. 7** Effect of chronic IOP on retinal histology and ganglion cell layer density evaluated after 15  
 629 weeks of IOP elevation. (a-d) Hematoxylin and eosin-stained retinal sections of a representative (a, c)  
 630 fellow control and (b, d) suture eyes in the peripheral (a, b) and central retina (c,d). (e) Cell density in  
 631 the GCL (cells/mm) in the peripheral retina, central retina and combined cell count (central and  
 632 peripheral) of sutured and fellow control eyes (n=7). Error bars: Standard deviation. Each circle in the  
 633 bar chart represents individual data points of the animals. \*  $p < 0.05$ , paired t-test. Scale bar: 100  $\mu\text{m}$ .

634



635 **Fig. 8**  $\beta$ -III-tubulin labeling of RGC after 15 weeks of IOP elevation: (a) Immunofluorescent staining  
 636 with anti- $\beta$ -III-tubulin and DAPI nuclear counterstained retinal sections of a representative control and  
 637 suture eye at week 15. (b) The RGC density (cells/mm) in the central retina of the control and sutured  
 638 eyes ( $n = 6$ ). Error bars: Standard deviation. Each circle in the bar chart represents individual data  
 639 points of the animals. \* $p < 0.05$ , paired t-test. Scale bar: 100  $\mu$ m.

640



641 **Fig. 9** Effect of chronic IOP on the optic nerve morphology evaluated after 15 weeks of IOP elevation.  
 642 The longitudinal sections of ON were stained with H&E to assess the structural alterations in axonal  
 643 bundles. Suture eyes with chronic IOP elevation (right column) resulted in posterior deformation of the  
 644 optic nerve head surface (\*). While the cell nuclei are lined up parallel to the axonal bundles in the  
 645 control optic nerve (left column), such arrangements appear altered in the sutured eyes with clustered  
 646 nuclei of cellular infiltrates (arrows) which are suggestive of activated microglia. Scale bar: 100  $\mu$ m.